TÜBİTAK

Research Article

Turkish J. Eng. Env. Sci.
35 (2011) , 69 – 82.

doi:10.3906/muh-1007-127

Production and characterization of porous TiNi shape memory alloys

Tarık AYDOĞMUŞ[1,*], **Ali Şakir BOR**[2]
[1]*Department of Mechanical Engineering, Yüzüncü Yıl University, 65080 Van-TURKEY*
e-mail: aydogmus@yyu.edu.tr
[2]*Department of Metallurgical and Materials Engineering, Middle East Technical University, 06531 Ankara-TURKEY*

Received: 15.07.2010

Abstract

In the present study, porous TiNi alloys (Ti-50.6 at. %Ni) with porosities in the range of 21%-26% were prepared, applying the conventional powder metallurgy fabrication route in which magnesium was used as the getter, resulting in a single austenite phase dictated by the composition of the starting prealloyed powders and entirely free from secondary brittle intermetallics, oxides, nitrides, and carbonitrides. Although porous TiNi alloys produced by conventional sintering have not been found to be appropriate for bone replacement applications involving bone ingrowth due to their small pore size (4-65 μm on average, depending on compaction pressure) and low porosity, they are appropriate for filtering applications due to their highly interconnected pore structures (over 90%), which provide excellent permeability. Since they meet the main mechanical requirements expected from an implant material, such as low Young's moduli, high strength, and ductility, they can also be used in the processing of metallic foams with gradient porosity.

Key Words: Porous TiNi, sintering, oxidation, superelasticity, shape memory alloys (SMA)

1. Introduction

TiNi shape memory alloys are reliable, functional materials widely used in various industrial applications as couplings, actuators, sensors, retractable antenna for mobile phones, glasses frames, and underwire for underwire bras due to their unique shape memory and superelasticity properties (Funakubo, 1987; Otsuka and Wayman, 1998). The combination of these characteristics with good biocompatibility (Shabalovskaya, 1996), coupled with high mechanical response, has made TiNi alloys fabulous materials for dental and biomedical applications such as stents, orthodontic arch wires, filters, and bone anchors (Itin et al., 1994; Pelton et al., 2000). The retention of TiNi features well enough also in the porous form, introducing new application fields including bone implants, energy absorbers, separators, and light weight actuators (Bansiddhi et al., 2008). Biomedical applications, especially bone implants, stay one step ahead of the others due to the high cost of porous TiNi alloys. Moreover, shape memory and superelasticity properties can easily be used practically for insertion of implants, ensuring

*Corresponding author

better fixation with the host tissue. Superelastic porous TiNi alloys also display a mechanical behavior similar to that of the bones, showing strain recovery around 2% (Gjunter et al., 1995). Therefore, they exhibit a better mechanical compatibility compared to rival porous materials made up of stainless steel, tantalum, titanium, Ti6Al4V, or ceramics such as hydroxyapatite. Porosity is of service in allowing transportation of body fluids and bone ingrowth, and also in decreasing the elastic modulus of the implant, which is usually much higher than that of compact bone (12-17 GPa) or cancellous bone ($<$3 GPa) (Gjunter et al., 1995). Thus, the stress-shielding effect resulting from elastic moduli mismatch between the bone and the implant material is minimized.

Several powder metallurgy methods have been used to produce porous TiNi alloys, such as self-propagating high temperature synthesis (SHS) (Li et al., 2000; Yuan et al., 2006; Kaya et al., 2009; Tosun et al., 2009), conventional sintering (CS) (Li et al., 1998; Zhu et al., 2005), hot isostatic pressing (HIP) (Lagoudas and Vandygriff, 2002; Greiner and Oppenheimer, 2005), metal or powder injection molding (MIM) (Grummon et al., 2003; Guoxin et al., 2008), spark plasma sintering (SPS) (Zhao et al., 2005), and the space holder technique (SHT) (Bansiddhi and Dunand, 2007; Wu et al., 2007; Zhang et al., 2007; Bansiddhi and Dunand, 2008; Aydoğmuş and Bor, 2009; Li et al., 2009). All of the processing efforts, except for one study (Aydoğmuş and Bor, 2009), resulted in multiphase foams, including Ti_2Ni, $TiNi_3$, and Ti_3Ni_4 intermetallics, besides the desired main TiNi solid solution. Formation of secondary phases in the case of elemental powder usage is unavoidable, since their formation is much more favorable thermodynamically compared to the formation of TiNi. Their removal is also very difficult once they come into existence. Secondary phases other than TiNi do not exhibit shape memory or superelasticity and also make the foam produced brittle. Only Ti_3Ni_4 precipitates are useful for improving shape memory and superelasticity characteristics when they are formed as coherent or semi-coherent precipitates by suitable aging heat treatments. Contamination (e.g. oxidation) during processing is another factor causing synthesized porous TiNi alloy to be brittle. Oxidation also triggers secondary phase formation in the case of prealloyed powder sintering (Krone et al., 2004; Schüller et al., 2005; Mentz et al., 2006). Secondary phases and contamination do not only affect mechanical properties, but they additionally change phase transformation temperatures, which are important for practical applications.

Prealloyed powder sintering under nonoxidizing atmosphere can prevent secondary phase formation and contamination and related brittle behavior. This paper investigates the sintering of prealloyed TiNi powders under magnesium atmosphere using conventional powder metallurgy processing. It also presents the microstructural, thermal, and mechanical characteristics of the produced porous TiNi alloys.

2. Experimental procedure

2.1. Materials used

Prealloyed, spherical TiNi powders (Ti-50.6 at. %Ni, 99.9% purity), shown in Figure 1a, were used to produce porous TiNi specimens, while spherical Mg powders (Figure 1b) (99.82% purity) were employed to provide a nonoxidizing atmosphere upon vaporization during sintering. The TiNi powders exhibited Gaussian (log-normal) particle size distribution with a mean diameter of 21 μ, while the particle size of the Mg powders was in the range of 250 to 600 μm, averaging 450 μm.The TiNi powders were completely austenitic at ambient temperature (22 $\pm$ 2 °C), as confirmed by X-ray diffraction (XRD) (Figure 2a) and scanning electron microscopy (SEM) (Figure 2b) techniques.

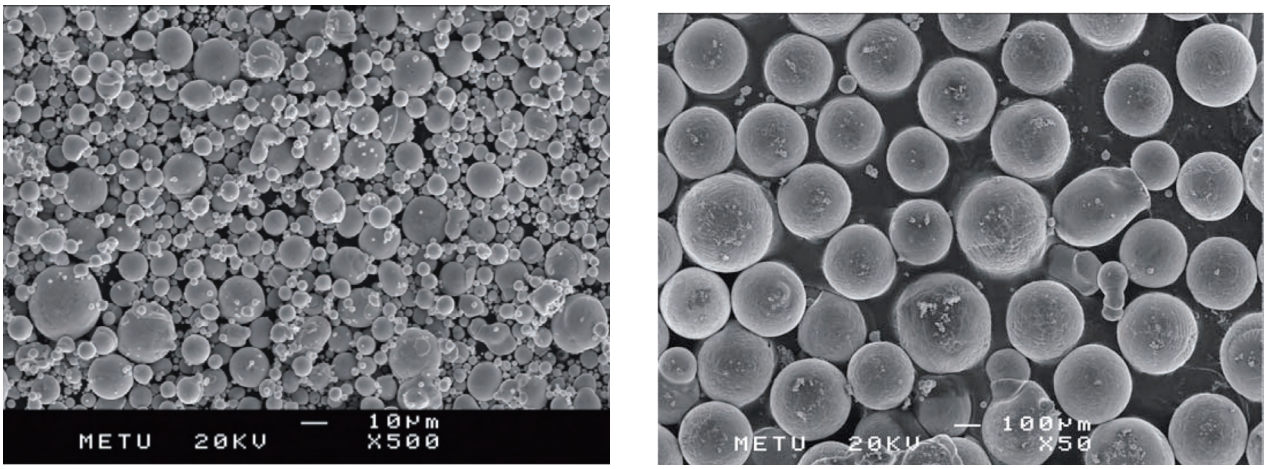

(a) (b)

Figure 1. SEM micrographs of initial powders: a) TiNi, b) Mg.

2.2. Production technique

The production method used in the present study was as follows: TiNi powders were blended using a 5% wt polyvinyl alcohol (PVA) solution (2.5% wt PVA + water) as the binder prior to compaction. Blended prealloyed TiNi powders and binder mixtures were consolidated in a double-ended steel die using a hydraulic press at a pressure of 770 MPa, which was determined to be optimum from preliminary experiments conducted at different pressures in the range of 190-1150 MPa. The amount of Mg added into the crucible alongside the compacted specimen before sintering was 12% of the weight of the TiNi compact. The sintering process was conducted at 1100 °C for 1 h in a purified argon atmosphere. Titanium was used as the getter to clean the Ar gas. Sintered porous specimens were cooled in the cold zone of the furnace at a rate of approximately 60-75 °C/min, sufficient to prevent formation of intermetallics other than TiNi due to possible oxidation problems that may occur during furnace cooling.

2.3. Heat treatment

A few samples were aged at 400 °C for 1 h under a protective, inert Ar gas atmosphere in a tube furnace subsequent to the sintering process. Solutionizing prior to aging was not required since preliminary experiments showed that the as-sintered samples did not contain secondary phases to be dissolved. Aging temperature and time employed were chosen on the basis of optimizing the superelastic properties, considering the literature survey results for bulk TiNi alloys with the same composition. To minimize the oxidation during aging, porous TiNi alloys were embedded in Mg powders before processing. Porous TiNi alloys held in the cold zone initially were placed into the hot zone of the furnace when it reached the aging temperature. After aging for 1 h at 400 °C, samples were moved again to the cold zone and cooled there for 3 min. They were then removed from the furnace and cooled by spraying alcohol onto them immediately. The total cooling time was less than 4 min. Quenching was not performed, since it results in considerable oxidation.

2.4. Characterization methods

Density and porosity content of the green compacts and porous TiNi specimens produced were determined employing Archimedes' principle. A Rigaku D/Max 2200/PC model X-ray diffractometer was used for phase

analysis. The pore characteristics and microstructure of the produced specimens were revealed using a JEOL JSM 6400 scanning electron microscope equipped with Noran System 6. Pore sizes were determined using a Quantachrome PoreMaster 60 mercury porosimeter. Phase transformation temperatures of the TiNi powders and porous TiNi alloys were measured with a PerkinElmer Diamond differential scanning calorimeter (DSC) through the temperature range of –60 to 150 °C, with a heating and cooling rate of 10 °C/min and under nitrogen atmosphere. Superelasticity tests were conducted cyclically at a constant stress of 380 MPa in compression at room temperature, using a 30-kN capacity Instron 3367 mechanical testing system at a constant crosshead speed of 0.1 mm/min, and cylindrical specimens of 10 mm in both diameter and height.

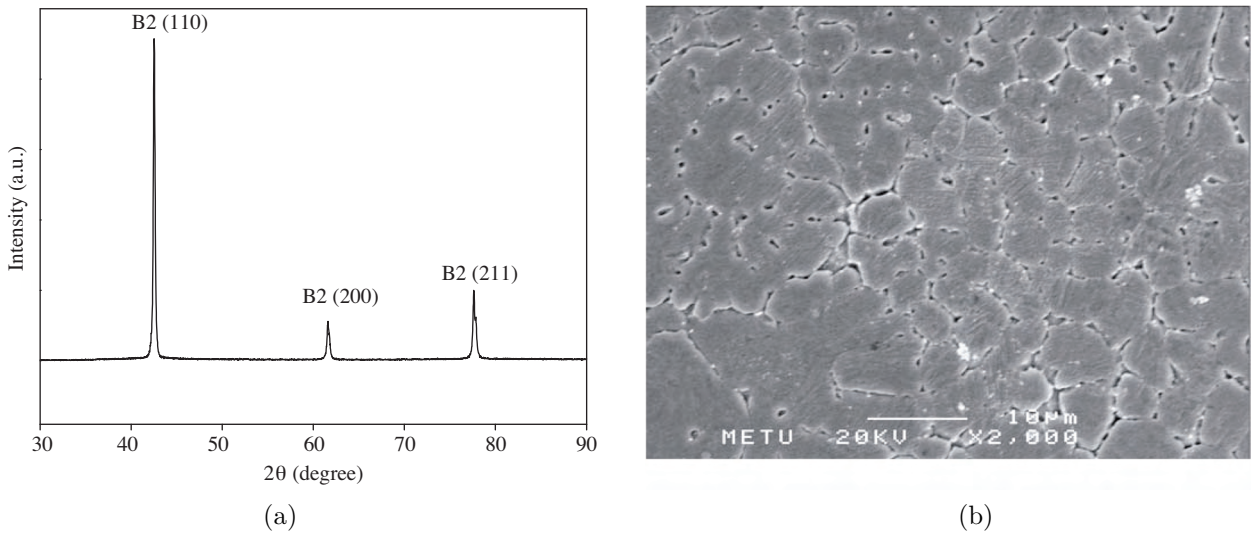

Figure 2. Microstructure of TiNi powders: a) XRD pattern showing ordered B2 austenite peaks, b) SEM micrograph indicating austenite dendrites in prealloyed TiNi powder produced by inert gas atomization.

3. Results and discussion

3.1. Porosity and pore characteristics of porous TiNi alloys

The effect of compaction pressure on green density and porosity is shown in Figure 3. The tap density of initial prealloyed TiNi powders was measured to be 4.195 g/cm^3 and the corresponding porosity was 34.96%. Application of pressure resulted in an increase in density and a decrease in porosity, as expected, and the maximum green density attained was 5.07 g/cm^3, corresponding to a porosity level of 22% after compaction at the maximum stress of 1150 MPa.

It is clear from Figure 3 that the compaction behavior of TiNi powders is similar to those of other prealloyed powders. The compaction operation starts with the rearrangement of the powders. Interparticle friction between powders dominates at this step and is controlled by the surface area, surface chemistry, and surface morphology or surface roughness of the powders. Since the TiNi powders used in the present study were so fine (20 μm on average), their surface areas were extremely large. Larger surface areas generally mean higher interparticle friction and lower packing, and also inadequate rearrangement. Subsequent to the initial rearrangement of powders, localized deformation occurs at powder contacts as pressure is applied. Increasing the pressure results in an increase in the relative volume of each particle undergoing plastic deformation. Further increases in pressure cause the elimination of more pores and the creation of new contacts, and finally

the homogeneous deformation of the whole compact. Work hardening inevitably comes along with plastic deformation, and higher density levels require higher external energy. The compressibility of TiNi powders has been found to be lower than that of conventional powders, and getting a durable, crack-free compact is also much more difficult due to the superelasticity during compaction. Austenitic TiNi powders subjected to a consolidation process (in which deformation occurs first by stress-induced martensite formation at up to 7% strain, and then dislocations) regained their shape, at least partially, due to superelasticity, as can be seen from Figure 4. At lower compaction pressures, all martensites formed during the compaction step transformed into austenite with the release of load. On the contrary, higher compaction pressures, such as 575 MPa, led to the stabilization of stress-induced martensites by introducing dislocations. Dislocations prevent the movement of mobile austenite/martensite interfaces, and as a result, shape recovery deteriorates. This undesired phenomenon of martensite stabilization under normal circumstances turns into a required condition for the compaction of superelastic TiNi alloy powders. Otherwise, sound green samples with lower porosity and sufficient green strength could not be produced. Thus, lower compaction pressures ($<$575 MPa) would not be sufficient to produce crack-free compacts. Compaction pressure was observed to not be a critical parameter in the production of samples 10 mm in diameter and 3 mm in height. However, among those tested in this study, specimens 10 mm in both diameter and height for compression testing were producible only using a pressure around 770 MPa. At 1150 MPa, although better green density was attained, ejection of compacted samples from the die was much more difficult, even when a lubricant such as zinc stearate was used. Both springback and superelasticity mechanisms obstructed easy ejection. Since the springback effect increases with approximately the square of the compaction pressure (German, 1994), it might be the dominating mechanism.

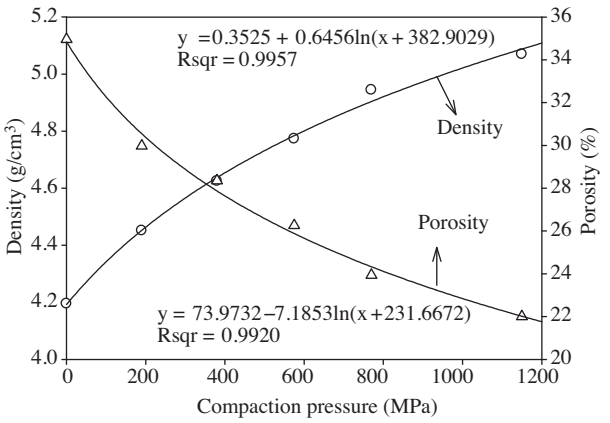

Figure 3. Density and porosity of compacts under different compaction pressures.

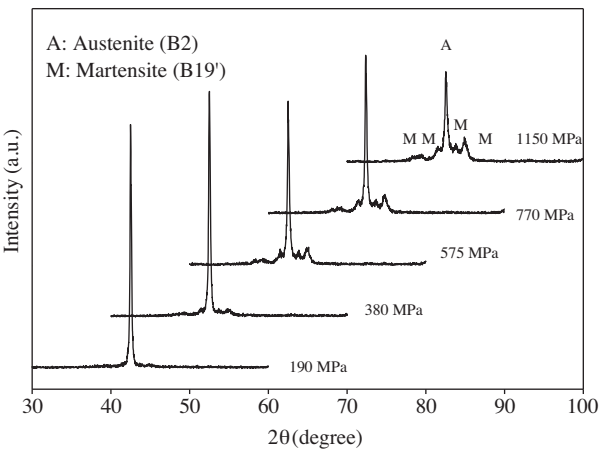

Figure 4. XRD pattern of green TiNi compacts obtained at different pressures; for clarity, peak positions were relatively shifted 10° to the right.

Powder shape, size, and distribution affect the interparticle friction, packing density, and pore size. Powders with a smaller particle size are more difficult to press. Log-normal particle size distribution leads to lower green densities. Instead, bimodal particle size distribution guarantees a better densification. Spherical powders are pressed more difficultly than irregular powders. Therefore, the spherical, fine powders used in the present study also effected densification adversely, but it was not of much concern since the aim of the present study was not to produce a TiNi shape memory alloy with minimum porosity. However, durable compacts in a

broad porosity range would be better. Nevertheless, adjustment of powder size, shape, and distribution allows a limited control on final porosity and mechanical properties.

Figure 5 presents the effect of compaction pressure on final (sintered) density and porosity contents. Upon sintering, a decrease in the range of 0.8%-3.7% was observed in the porosity content of the compacts. Sintering shrinkage was lower than 2% in diameter for all of the samples produced, while up to 2% swelling was observed in height. The swelling observed in height resulted from the strain recovery of the TiNi compacts by the shape memory mechanism during heating, rather than the conventional swelling that occurs frequently in elemental powder sintering of TiNi alloys.

Porosity distribution of sintered TiNi alloys compacted at different pressures is presented in Figure 6. It can be seen that pore size decreased with increasing compaction pressure. Mean pore size corresponding to 50% cumulative was found to decrease from 65 μm for the lowest pressure applied, 190 MPa, to approximately 4 μm for the highest pressure of 1150 MPa. The largest pore size observed was around 200 μm. Biomedical applications require pore sizes in the range of 100-600 μm for bone tissue ingrowth (Itin et al., 1994). Therefore, porosity content with pore sizes larger than 100 μm is an important parameter. A compaction pressure of 190 MPa assured that 40% of the total porosity was larger than 100 μm. This rate decreased to 20% for 380 and 575 MPa, while it was around only 5%-6% for higher pressures. However, such large pore sizes (e.g. 100 μm and higher) were not observed in SEM analysis (Figure 7), probably because these were interconnected pores that cannot be sampled in polished specimens.

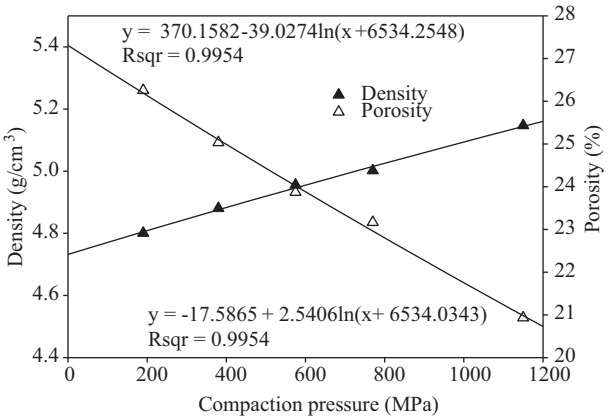

Figure 5. Density and porosity of porous TiNi alloys after sintering as a function of compaction pressure applied during consolidation.

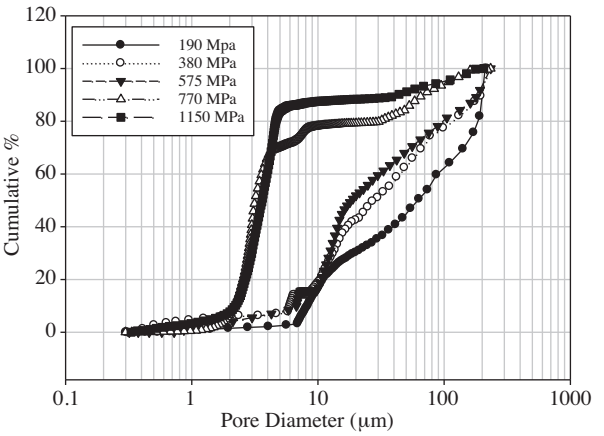

Figure 6. Porosity distribution in sintered porous TiNi alloys as a function of compaction pressure.

It is apparent from Figure 7 that pore shape in porous TiNi alloys produced by conventional sintering is irregular. In general, pores in a porous material or in a foam can be classified as open pores, which are connected to the external surface of the porous sample, and closed pores (also defined as isolated pores), which are not connected to the external surface of the material. Almost all of the pores resulting from low packing of the initial powders, low compaction pressures, and pressureless partial sintering in conventionally sintered samples were the interconnected and open type. Some isolated or closed pores were also observed during SEM investigations, as clearly seen in Figure 7. The majority of these pores were located at the interior of the powders. It is highly probable that isolated pores in the powders were formed during the atomization process.

Incomplete densification of cell walls also may have created some closed, finer pores, contributing to general closed porosity.

The open pore rate, i.e. the rate of open porosity to total porosity in percentage, for sintered porous TiNi samples conventionally cold compacted at different pressures was greater than 90%. Since the open pore rate was quite high, it was difficult to distinguish the pore geometry and size metallographically using the image analyzer. Moreover, to obtain a reasonable and accurate pore size distribution, the image analysis method was found to not be appropriate due to irregular pore shapes and high connectivity.

It should be noted that general porosity (i.e. total porosity), open pore rate, and pore size are very important factors for biomedical applications, especially for bone implantation, because a sufficient porosity with a high open pore rate allows natural bone regrowth to occur until complete intimate contact has been achieved between the bones and the porous implants. Pores should be interconnected, giving a minimum open porosity of 30% for bone ingrowth and body fluid transportation, while porosity should be in the range of 30%-90% for bone replacement applications (Bansiddhi et al., 2008). The pore size requirement, as mentioned before, is 100-600 μm. Porous TiNi alloys fabricated by the classical cold compaction and sintering method, with porosities in the range of 21%-26% (lower than the required 30%) and average pore sizes in the range of 4-65 μm, are not suitable for artificial bone implants. On the other hand, they are appropriate for filtering applications due to their highly interconnected pore structures, which provide excellent permeability.

3.2. Macro- and microstructure

The SEM image given in Figure 8 displays the macro view of the porous TiNi alloy in the as-sintered condition. It was recognized that magnesium powders initially directly touching the consolidated TiNi surface got stuck there during sintering, upon reacting with oxygen in the medium, forming magnesium oxide particles a few micrometers (up to 5 μm) in size (Figure 9). In contrast, the surface regions not initially in direct contact with the magnesium powder were found to be free of magnesium or magnesium oxide after sintering.

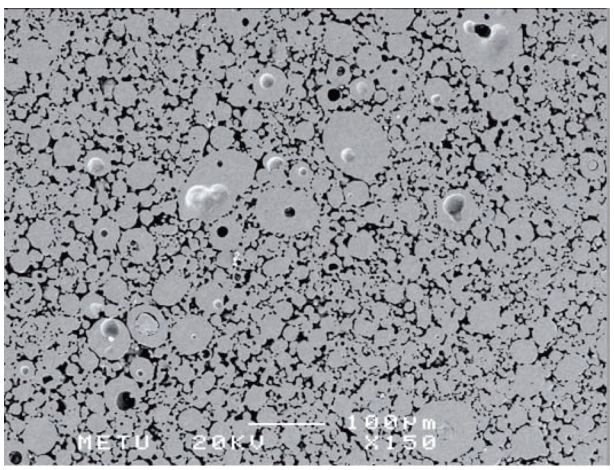

Figure 7. SEM micrograph of sintered TiNi alloy with 23% porosity (compaction pressure: 770 MPa).

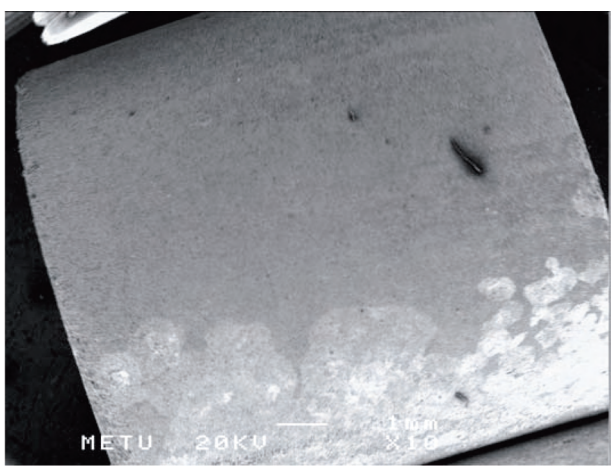

Figure 8. SEM picture showing residual MgO layer coated onto porous TiNi alloy during sintering operation.

Magnesium melts at 650 °C and its vapor pressure starts to increase drastically in the liquid state with increasing temperature. The temperature rise also accelerates the magnesium oxidation reaction. Liquid magnesium wets the TiNi compact surface and reduces the oxide of TiNi powders while reacting with the

residual oxygen of the furnace atmosphere in the crucible. As a result, magnesium oxide particles form on the surface of porous TiNi intensely, but solely on the regions in direct contact with magnesium powders before sintering. It was also observed that liquid magnesium erodes the TiNi compact surface to some degree, which is clearly noticeable in Figure 9.

Figure 10 shows a SEM micrograph, taken at a higher magnification, of the clean surface (not contacted by magnesium powders initially) of sintered porous TiNi. Areal EDX analysis in this region indicated only 2.3% wt residual magnesium. The residual magnesium oxide particles present on the powders or sintering necks, shown with black arrows in Figure 10, were smaller than 2.5 μm. No sign of erosion was observed because these surface regions were subjected to merely vaporized magnesium. Interior regions of the produced porous TiNi alloys were completely free of magnesium and magnesium oxide particles.

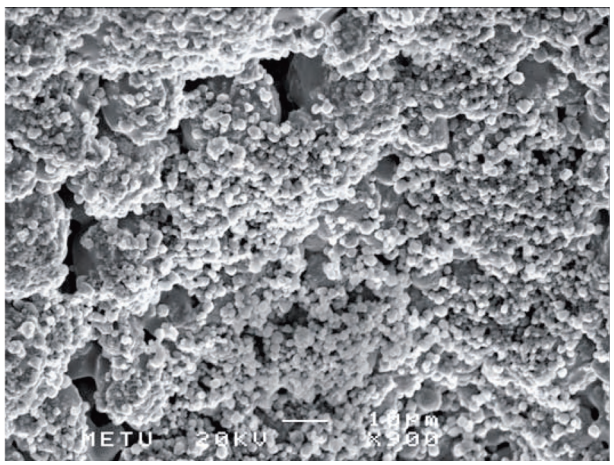

Figure 9. SEM micrograph indicating residual MgO particles on sintered TiNi powders.

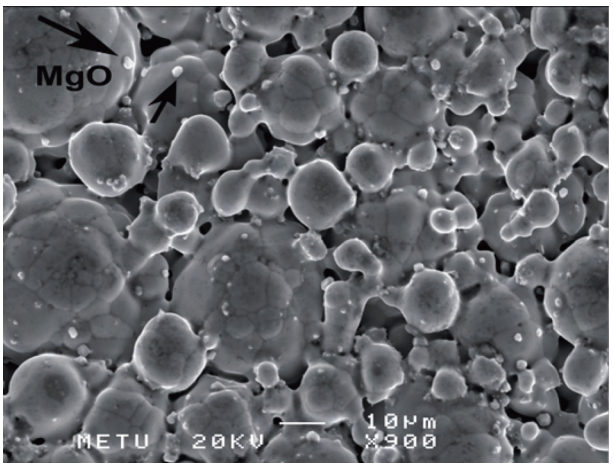

Figure 10. SEM image showing MgO particles condensed onto sintered TiNi powders.

In order to prevent the erosion of the TiNi compact by liquid magnesium and to minimize residual MgO particles over the surface, compacts were placed onto tall MgO pellets and the magnesium powders around the MgO pellets before sintering. Thus it was guaranteed that no part of the compact was in contact with magnesium powders. This design allowed the production of porous TiNi alloys with minimized residual magnesium oxide particles. Figure 11 presents the sample processed using the improved design. There were no MgO particles visible to the naked eye or stereomicroscope anywhere on the sample surface.

XRD patterns of the as-sintered porous TiNi SMAs previously compacted at various pressures are shown in Figure 12. Neither undesired secondary Ti-Ni intermetallics nor contamination compounds such as oxides, carbides, or carbonitrides of titanium or magnesium were detected. Single B2 austenite TiNi was the only phase present in all of the samples. The SEM micrograph displayed in Figure 13 also confirms the retention of the single B2 austenite phase after the sintering operation. Figure 13 also shows boundaries of grains formed in austenitic TiNi with a size of around 5-15 μm. It is clear that only the initial stage of sintering was achieved during processing. Individual powders were easily distinguishable from each other and large curvatures were quite explicit. Both neck size ratio (<0.3) and shrinkage (solely in diameter, 1.4%) were small and the grain size was found to be no larger than the initial particle size, 20 μm.

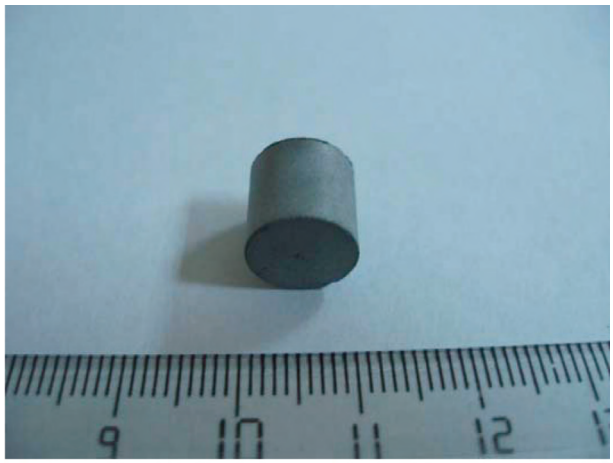

Figure 11. Macrograph of sintered TiNi compact without residual MgO.

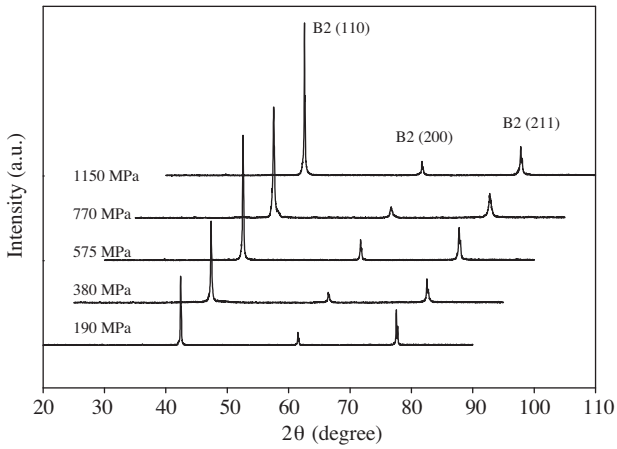

Figure 12. XRD spectra of sintered porous TiNi alloys; for clarity, peak positions were shifted 5° to the right beyond 190 MPa.

As a result of aging treatment at 400 °C for 1 h, Ti_3Ni_4 precipitates formed in the austenitic TiNi matrix of porous TiNi alloys can be seen from the XRD pattern given in Figure 14. Since the coherent precipitates expected to form by this heat treatment are only a few tens of nanometers in size (Otsuka and Ren, 2005), they were not observed under SEM.

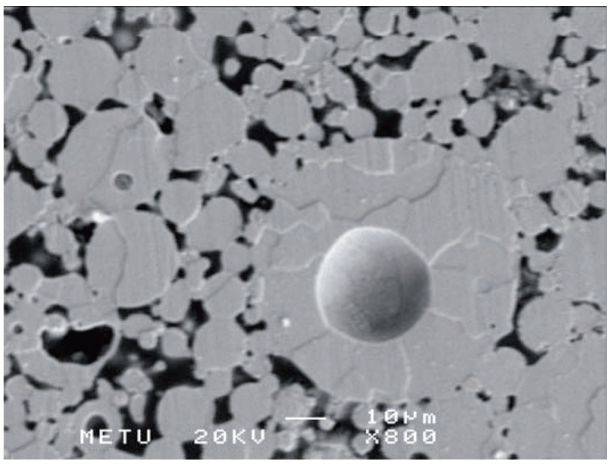

Figure 13. Microstructure of porous TiNi with a porosity of 23%, showing austenite grain boundaries.

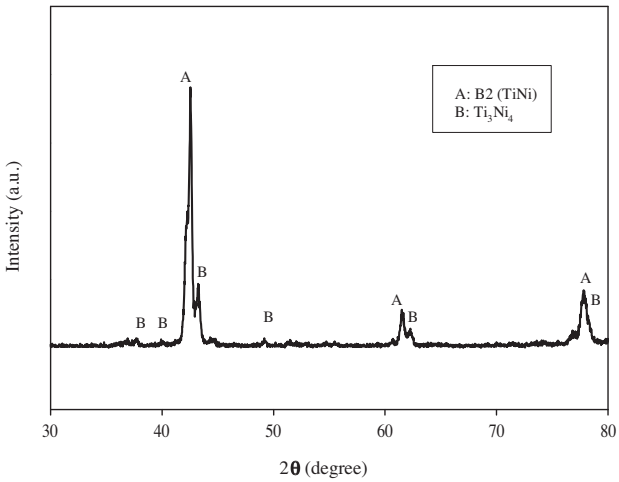

Figure 14. XRD pattern of aged porous TiNi at 400 °C for 1 h.

3.3. Phase transformation behavior in porous TiNi alloys

Figure 15 represents the typical DSC curves of the raw powder used, porous TiNi sintered at 1100 °C for 1 h, and porous TiNi aged at 400 °C for 1 h after sintering at the same conditions. Raw prealloyed TiNi powders showed broad austenite and martensite peaks during heating and cooling, and as a result the martensite start (M_s), martensite peak (M_p), martensite finish (M_f), and austenite start (A_s) temperatures could not be determined precisely. This may have arisen from the compositional inhomogeneities of the powders formed

during the atomization process. It is well known that Ni content plays an important role in phase transformation temperatures, and local regions with varying Ni content in the powders will transform at different temperatures, which will result in a broad transformation peak. The second peak observed in the cooling curve cannot be attributed to the R-phase, since the Ti_3Ni_4 precipitate phase that assists R-phase formation was not present (as confirmed by XRD). This second peak probably also originated from local deviations in Ni content. As-sintered porous TiNi alloy, on the other hand, exhibited a single distinct peak during both heating and cooling as a result of compositional homogenization during sintering. Transformation temperatures of as-sintered porous TiNi were slightly higher than those of the raw powder, as can be seen from Figure 15 and Table 1, due to homogenization and reduction of oxides by magnesium getters during the sintering process. Aging treatment caused an additional increase in phase transformation temperatures; A_s and A_f temperatures were found to be 16 and 65 °C, respectively, whereas M_s and M_f were measured as 62 and 4 °C, respectively. The areas under the martensite and austenite peaks (i.e. latent heat of forward and reverse transformations) were only 4.5 and 7.1 J/g, respectively. It was reported in a previous study that a melt-cast TiNi alloy of the same Ni content (50.6 at. %) had a forward transformation latent heat of around 25 J/g (Otubo et al., 2008). This suggests that nontransforming phases, e.g. Ti_3Ni_4, were present in the sample. It is peculiar that although the M_s and M_f temperatures were 62 and 4 °C, respectively, and the XRD studies were carried out around 25 °C, the XRD spectrum (Figure 14) of aged specimens did not display a B19' martensite phase peak, which is expected at room temperature beside Ti_3Ni_4 precipitates.

Table 1. Phase transformation temperatures and corresponding latent heats of transformations of prealloyed TiNi powders and porous TiNi samples in as-sintered and aged conditions.

Condition	Phase transformation temperatures (°C)						Latent heat of transformations ΔH, J/g	
	M_s	M_p	M_f	A_s	A_p	A_f	$-\Delta_{forw}$	Δ_{rev}
Powder	10	-25	-53	-11	20	30	14.4	13.8
As-sintered	16	4	-39	8	35	41	18.0	17.0
Aged	62	49	4	16	54	65	4.5	7.1

3.4. Mechanical and superelasticity properties

Compression stress-strain curves of as-processed (as-sintered), as-quenched, and aged porous TiNi alloys with a porosity content of 23% are presented in Figure 16. The as-quenched sample displayed the highest strength due to severe oxidation occurring during rapid cooling from 1100 °C to room temperature, using water at ambient temperature as the cooling medium. Oxidation might also trigger lower martensitic transformation temperatures. Since all of the mechanical tests were carried out at the same temperature, room temperature, the sample with the lowest transformation temperatures would be the strongest. Mechanical properties of the aged sample were between those of the as-processed and as-quenched samples. Table 2 lists the elastic moduli, critical stress required for inducing martensite, and compressive strength values quantitatively obtained from the stress-strain diagram. It is clear that while strength improved and unrecovered strains decreased with cycling, especially after the first cycle, elastic moduli values stayed at almost the same level. It was also noted that unloading elastic moduli were not very different from those calculated from the loading curves. Another observation was related to linear superelasticity behavior after the cycling process. All 3 samples in

different conditions showed incomplete strain recovery in the first cycle. Irrecoverable strains were 1.16% for the as-quenched sample, 1.46% for the aged sample, and 1.7% for the as-processed sample. The existence of nonrecoverable strains is owing to 2 reasons: one is that the A_f temperatures were higher than room temperature and the other is that the irregular shape of the pores easily causes stress concentration, which results in irrecoverable deformation.

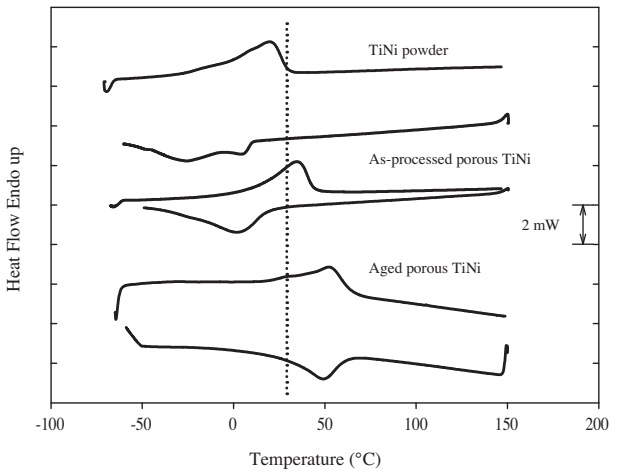

Figure 15. DSC curves of TiNi powder, as-sintered porous TiNi, and subsequently aged porous TiNi (porosity 23%).

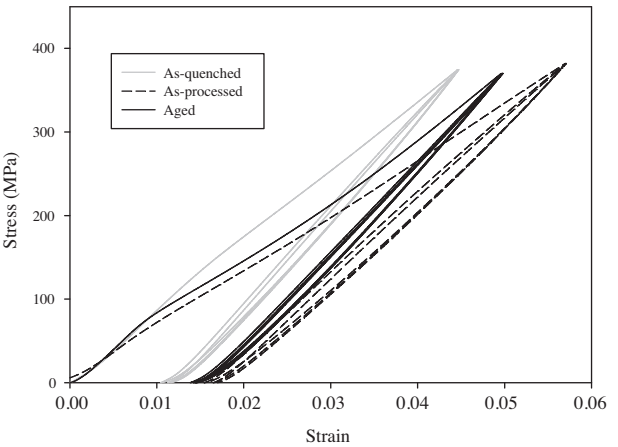

Figure 16. Stress-strain curves of porous TiNi in as-quenched, as-processed, and aged conditions (porosity 23%).

Table 2. Mechanical properties of porous TiNi alloys in various conditions.

Sample	Young's modulus (E, GPa)	Critical stress for inducing martensite (σ_{cr}, MPa)	Compressive strength at 2% strain ($\sigma_{\max}$, MPa)		
			First cycle	Second cycle	Third cycle
As-quenched	17	161	176	216	220
As-processed	13.2	140	135	186	188
Aged	16.8	112	146	198	199

Although porous TiNi alloys produced by conventional sintering have not been found to be appropriate for bone replacement applications due to their unsuitable pore size and pore amount, there was no problem detected in terms of their mechanical properties. They already meet the main requirements, including high strength, low elastic modulus, and strain recovery ability, expected from an implant material. In this sense, they can easily be used in producing metallic materials for gradient porosity applications. For example, they can be used in hard tissue replacement material as the denser core of the implant. While the high porosity and large pores at the outer surface would allow and promote tissue cell ingrowth, the dense core inside the implant material would be capable of bearing loads and strain recovery. Porous TiNi is better than bulk TiNi because it provides for transportation of body fluids through its micropores. Moreover, it is sufficient in strength and toughness and has a lower elastic modulus value. Thus, the stress-shielding effect may also be minimized.

4. Conclusions

Prealloyed Ni-rich Ti-50.6 at. %Ni powders were conventionally sintered at 1100 °C for 1 h to produce porous TiNi alloys under magnesium vapor, which was used as the oxygen getter, leading to the following conclusions.

1. Magnesium vapor effectively protects porous TiNi samples from contamination and prevents secondary phase formation during sintering operations. The room temperature microstructure of the samples produced was a single austenite phase entirely free from secondary brittle intermetallics, oxides, nitrides, and carbonitrides.

2. Specimens produced by conventional sintering exhibited irregular open pores with an average size of 4-65 μm and porosities in the range 21%-26%, depending on the compaction pressure and initial powder size. The produced porous TiNi alloys were not appropriate for bone replacement applications due to their small pore size and low porosity content. However, they seem to be appropriate for filtering applications due to their highly interconnected pore structures.

3. Martensitic transformation temperatures were observed to increase after sintering due to homogenization and reduction of oxides by magnesium getters. Aging treatment, resulting in formation of coherent Ti_3Ni_4 precipitates, also increased the phase transformation temperatures.

4. Unlike the bulk ones, porous TiNi alloys show linear superelasticity after the cycling process. Strength improves and unrecovered strains decrease with cycling. The existence of nonrecoverable strains is owing to 2 reasons: one is that the A_f temperatures are higher than room temperature and the other is that the irregular shape of the pores easily causes stress concentration, which results in irrecoverable deformation.

Acknowledgment

This research was supported partly by the Scientific and Technological Research Council of Turkey (TÜBİTAK) under Grant No. 108M118.

References

Aydoğmuş, T. and Bor, Ş., "Processing of Porous TiNi Alloys Using Magnesium as Space Holder", Journal of Alloys and Compounds, 478, 705-710, 2009.

Bansiddhi, A. and Dunand, D.C., "Shape-Memory NiTi Foams Produced by Solid-State Replication with NaF", Intermetallics, 15, 1612-1622, 2007.

Bansiddhi, A. and Dunand, D.C., "Shape-Memory NiTi Foams Produced by Replication of NaCl Space-Holders", Acta Biomaterialia, 4, 1996-2007, 2008.

Bansiddhi, A., Sargeant, T.D., Stupp, S.I. and Dunand, D.C., "Porous NiTi for Bone Implants: A Review", Acta Biomaterialia, 4, 773-782, 2008.

Funakubo, H., Shape Memory Alloys, Gordon and Breach Science Publishers S.A., Amsterdam, 1987.

German, R.M., Powder Metallurgy Science, Metal Powder Industries Federation, New Jersey, 1994.

Gjunter, V.E., Sysoliatin, P. and Temerkhamor, T., Superelastic Shape Memory Implants in Maxillofacial Surgery, Traumatology, Orthopaedics, and Neurosurgery, Tomsk University Publishing House, Tomsk, 1995.

Greiner, C., Oppenheimer, S.M. and Dunand, D.C., "High Strength, Low Stiffness, Porous NiTi with Superelastic Properties", Acta Biomaterialia, 1, 705-716, 2005.

Grummon, D.S., Shaw, J.A. and Gremillet, A., "Low-Density Open-Cell Foams in the NiTi System", Applied Physics Letters, 82, 2727-2729, 2003.

Guoxin, H., Lixiang, Z., Yunliang, F. and Yanhong, L., "Fabrication of High Porous NiTi Shape Memory Alloy by Metal Injection Molding", Journal of Materials Processing and Technology, 206, 395-399, 2008.

Itin, V., Gyunter, V., Shabalovskaya, S. and Sachdeva, R., "Mechanical Properties and Shape Memory of Porous Nitinol", Materials Characterization, 32, 179-187, 1994.

Kaya, M., Orhan, N., Kurt, B. and Khan, T.I., "The Effect of Solution Treatment under Loading on the Microstructure and Phase Transformation Behavior of Porous NiTi Shape Memory Alloy Fabricated by SHS", Journal of Alloys and Compounds, 475, 378-382, 2009.

Krone, L., Schüller, E., Bram, M., Hamed, O., Buchkremer, H.P. and Stöver, D., "Mechanical Behaviour of NiTi Parts Prepared by Powder Metallurgical Methods", Materials Science and Engineering A, 378, 185-190, 2004.

Lagoudas, D.C. and Vandygriff, E.L., "Processing and Characterization of NiTi Porous SMA by Elevated Pressure Sintering", Journal of Intelligent Materials Systems and Structures, 13, 837-850, 2002.

Li, B., Rong, L.J. and Li, Y.Y., "Porous NiTi Alloy Prepared from Elemental Powder Sintering", Journal of Materials Research, 13, 2847-2851, 1998.

Li, B.Y., Rong, L.J., Li, Y.Y. and Gjunter, V.E., "Synthesis of Porous Ni-Ti Shape-Memory Alloys by Self-Propagating High-Temperature Synthesis: Reaction Mechanism and Anisotropy in Pore Structure", Acta Materialia, 48, 3895-3904, 2000.

Li, D.S., Zhang, Y.P., Eggeler, G. and Zhang, X.P., "High Porosity and High-Strength Porous NiTi Shape Memory Alloys with Controllable Pore Characteristics", Journal of Alloys and Compounds, 470, L1-L5, 2009.

Mentz, J., Bram, M., Buchkremer, H.P. and Stöver, D., "Improvement of Mechanical Properties of Powder Metallurgical NiTi Shape Memory Alloys", Advanced Engineering Materials, 8, 247-252, 2006.

Otsuka, K. and Ren, X., "Physical Metallurgy of Ti-Ni-Based Shape Memory Alloys", Progress in Materials Science, 50, 511-678, 2005.

Otsuka, K. and Wayman, C.M., Shape Memory Materials, Cambridge University Press, Cambridge, 1998.

Otubo, J., Rigo, O.D., Coelho, A.A., Neto, C.M. and Mei, P.R., "The Influence of Carbon and Oxygen Content on the Martensitic Transformation Temperatures and Enthalpies of NiTi Shape Memory Alloy", Materials Science and Engineering A, 481-482, 639-642, 2008.

Pelton, A.R., Stoeckel, D. and Duerig, T.W., "Medical Uses of Nitinol", Materials Science Forum, 327-328, 63-70, 2000.

Schüller, E., Krone, L., Bram, M., Buchkremer, H.P. and Stover, D., "Metal Injection Molding of Shape Memory Alloys Using Prealloyed NiTi Powders", Journal of Materials Science, 40, 4231-4238, 2005.

Shabalovskaya, S., "On the Nature of Biocompatibility and Medical Applications of Shape Memory and Superelastic NiTi-Based Alloys", Bio-Medical Materials and Engineering, 6, 267-289, 1996.

Tosun, G., Ozler, L., Kaya, M. and Orhan, N., "A Study on Microstructure and Porosity of NiTi Alloy Implants Produced by SHS", Journal of Alloys and Compounds, 487, 605-611, 2009.

Wu, S., Chung, C.Y., Liu, X., Chu, P.K., Ho, J.P.Y., Chu, C.L., Chan, Y.L., Yeung, K.W.K., Lu, W.W., Cheung, K.M.C. and Luk, K.D.K., "Pore Formation Mechanism and Characterization of Porous NiTi Shape Memory Alloys Synthesized by Capsule-Free Hot Isostatic Pressing", Acta Materialia, 55, 3437-3451, 2007.

Yuan, B., Zhang, X.P., Chung, C.Y., Zeng, M.Q. and Zhu, M., "A Comparative Study of the Porous TiNi Shape-Memory Alloys Fabricated by Three Different Processes", Metallurgical and Materials Transactions, 37A, 755-761, 2006.

Zhang, Y.P., Li, D.S. and Zhang, X.P., "Gradient Porosity and Large Pore Size NiTi Shape Memory Alloys", Scripta Materialia, 57, 1020-1023, 2007.

Zhao, Y., Taya, M., Kang, Y.S. and Kawasaki, A., "Compression Behavior of Porous NiTi Shape Memory Alloy", Acta Materialia, 53, 337-343, 2005.

Zhu, S.L., Yang, X.J., Fu, D.H., Zhang, L.Y., Li, C.Y. and Cui, Z.D., "Stress-Strain Behavior of Porous NiTi Alloys Prepared by Powders Sintering", Materials Science and Engineering A, 408, 264-268, 2005.